Available online at www.sciencedirect.com
SCIENCE DIRECT®
Surface Science 545 (2003) 47–69
SURFACE SCIENCE
www.elsevier.com/locate/susc

Adsorption and desorption of CO on Pt(1 1 1): a comprehensive analysis

J.-S. McEwen [a], S.H. Payne [a], H.J. Kreuzer [a,*], M. Kinne [b], R. Denecke [b], H.-P. Steinrück [b]

[a] Department of Physics and Atmospheric Science, Dalhousie University, Halifax, Nova Scotia, Canada B3H 3J5
[b] Physikalische Chemie II, Universität Erlangen-Nürnberg, Egerlandstr. 3, 91058 Erlangen, Germany

Received 16 June 2003; accepted for publication 26 August 2003

Abstract

A comprehensive theory of the adsorption of CO on Pt(1 1 1) is developed to describe equilibrium properties as well as the adsorption and desorption kinetics. The basis is a multi-site lattice gas model which allows for adsorption at on-top and bridge sites, and includes site exclusion and lateral interactions out to second neighbour unit cells as well as a mean field to account for long ranged dipolar interactions between CO molecules. The theory reproduces the coverage and temperature dependence of pressure isotherms, partial coverages, heat of adsorption, total sticking coefficients, and isothermal and temperature-programmed desorption rates. The quality of the fits and the internal consistency of the theory are such that a number of minor inconsistencies in available experimental data can be identified and discussed.

Keywords: Equilibrium thermodynamics and statistical mechanics; Models of surface kinetics; X-ray photoelectron spectroscopy; Adsorption kinetics; Sticking; Thermal desorption; Platinum; Carbon monoxide

1. Introduction

The adsorption of CO on Pt(1 1 1) is now a classical adsorbate system that has been studied for several decades by many techniques, to the extent that a large number of diverse data are available, both on equilibrium properties and also on the kinetics. It is the intention of this paper to develop a comprehensive theoretical framework in which all these data can be explained within the same model, namely a multi-site lattice gas model with multiple lateral interactions.

We begin with a summary of the experimental data; details and actual data will be given in sections on results. CO adsorbs on both on-top and bridge sites of Pt(1 1 1), with several ordered structures occurring depending on coverage and temperature. At low temperature (~100 K) Steininger et al. [1] observed superstructures with a $(\sqrt{3}\times\sqrt{3})R30°$ pattern at coverages of 0.17, 0.22, 1/3 ML and merging into a single diffuse $(\sqrt{3}\times\sqrt{3})R30°$ pattern around 150 K. Other groups have observed superstructures [2,3] and the diffuse pattern [4,5]. As coverage and temperature increase a $c(4\times 2)$ pattern appears around 0.35 ML,

* Corresponding author. Tel.: +1-902-494-6594; fax: +1-902-494-5191.
E-mail address: h.j.kreuzer@dal.ca (H.J. Kreuzer).

0039-6028/$ - see front matter © 2003 Elsevier B.V. All rights reserved.
doi:10.1016/j.susc.2003.08.040

becoming sharpest at 1/2 ML and 260–270 K [1,4]; for long exposures the coverage rises further to saturate around 2/3 ML. Compressed structures are observed in this region [1,6–9].

There have been many investigations of the frequencies of vibrational modes of CO (IRAS, EELS, TEAS) and hence binding sites [1,3,5,9–16], although not all studies are in agreement. The overall picture is that at low temperature and coverage the ordered patterns are due to CO occupying top sites predominantly and, with rising coverage and temperature, bridge sites become increasingly occupied. At 1/2 ML and for an annealed adlayer [1,17], the partial coverages of on-top and bridge-species are equal. Currently accepted mode frequencies are summarized by Hähner et al. [14].

Data on isotherms and isobars is limited. In early work by Ertl et al. [4], with coverages up to 0.7 ML, LEED patterns were used to calibrate coverage-pressure data from which heats of adsorption were derived. They found values around 138 kJ/mol at zero coverage, decreasing monotonically with coverage. Using He beam scattering, Poelsema et al. [18] obtained featureless isotherms in the pressure range 10^{-9}–10^{-6} mbar and for temperatures from 400 to 450 K, resulting in coverages less than 0.14 ML. A similar value for the zero-coverage heat of adsorption can be deduced. However, direct measurement of the heat of adsorption by Yeo et al. [19], using a microcalorimeter method, resulted in a significantly higher value of 180 kJ/mol; this decreased to about 80 kJ/mol at saturation. The first quantification of site partial coverages as a function of coverage and temperature was by Mieher et al. [9], using time resolved EELS, in an attempt to determine the site enthalpy difference.

Froitzheim's group [13,15] determined the adsorption kinetics directly by measuring the time evolution of site coverages in EELS. Most recently, high-resolution XPS studies [20] have determined the adsorption kinetics for a range of substrate temperatures (100–330 K) and pressures (varying by two orders of magnitude); from these data the sticking coefficient can be determined directly as a function of temperature and total CO coverage; additional data from these experiments will be presented here. The behaviour of the sticking is similar to that determined from coverage-dose curves obtained in several other studies [1,4,11,21], namely an initially constant value between about 0.5–0.9 up to coverages of 0.2–0.4 ML, followed by a roughly linear decrease to small values, around 10^{-3}, at 1/2 ML. Other measurements, around 300 K, have the sticking decreasing steadily in the range 0–1/2 ML [19,22].

The desorption kinetics has also been studied by many groups but with varying quality of results. As for some vibrational studies, early TPD studies showed the effects of defect adsorption sites [4,5, 22–24]. Defect-free surface TPD spectra [1,21,25, 26] exhibit a steady downward shift of the peak temperature with increasing initial coverage and, with one exception [1], these spectra are featureless with no indication of the adsorbate ordering or distinct site occupancy observed at adsorption temperatures. One study of isothermal desorption exists [20]. The question of the mobility of CO molecules at adsorption temperatures, and hence adsorbate equilibration times, is a controversial issue. Barriers to diffusion and attempt frequencies, determined by monitoring the evolution of CO site occupancy by He scattering [27,28] and RAIRS [29–31], cover a range of values. The more recent studies imply that CO is mobile above 100 K and this result is supported by the recent observation of flux-independence of the partial coverages, as a function of total coverage, for such temperatures [20].

A number of phenomenological models [9,12, 15,20] have been proposed to explain subsets of these experimental facts. They typically ignore other aspects of the system or are even in contradiction to known results and, as such, they lack consistency and should be taken as convenient parameterizations of data rather than attempts to understand the underlying dynamics of the adsorbate system. We will discuss these models in the context of the theory to be presented in this paper.

Quantum mechanical calculations of the geometry and energetics of the adsorption of CO on Pt(1 1 1) have a long history with a first comprehensive picture developed by Blyholder [32], in which binding occurs via a charge transfer from

the 5σ orbital of CO to the metal and a backdonation from the metal into the antibonding $2\pi^*$ orbital of CO. Although experimental evidence favors adsorption at low coverage at the on-top site, density functional calculations have consistently produced a preference for threefold hollow sites, as recently discussed at length by Feibelman et al. [33]. A solution to this persistent problem seems now to have been found by the inclusion of relativistic effects [34], although calculated binding energies still disagree, markedly, from experimental estimates.

In this paper we shall describe the adsorption and desorption of CO on Pt(1 1 1) within a multi-site lattice gas model which accounts for CO molecules at on-top, bridge and threefold hollow binding sites and lateral interactions between these. The theory we present entails more than the equilibrium properties of the adsorbate; by including the extension to a kinetic lattice gas model we formulate the direct and precursor-mediated adsorption kinetics properly. Because surface diffusion is fast, on the time scales of adsorption and desorption, quasi-equilibrium of the adsorbate is maintained and formulas for the sticking coefficients are explicit functions of coverage and temperature. This condition also permits non-equilibrium thermodynamics to be used for the description of the desorption kinetics, resulting in desorption rates which depend on these sticking coefficients and the activity of the adsorbate. The result is a comprehensive theory of CO on Pt(1 1 1), as regards equilibrium properties and kinetics.

In the next section we introduce the lattice gas model, briefly. In Section 3 we consider the equilibrium properties of the adsorbate. We describe our methods of calculation and use the theory to fit the available data on the system, such as adsorption isotherms and partial coverages, thus fixing the parameters of the lattice gas model. Section 4 deals with the adsorption kinetics. We introduce the pertinent aspects of precursor-mediated sticking and then use the lattice gas model, together with our data on the time-evolution of the site partial coverages, to calculate the site-dependent sticking coefficients. In Section 5 we calculate desorption spectra and show that the experimental rates follow, without significant adjustments, from our model and knowledge of equilibrium and adsorption data. Lastly, we discuss the phenomenological models advanced by previous authors and some of the contradictions in experimental data. The paper ends with a summary of what has been achieved.

2. Multi-site lattice gas model

The potential energy surface of an adparticle above a surface varies throughout a unit cell with local minima that represent energetically preferred adsorption sites, provided that the residence time of an adparticle in one of these sites is long compared to the time it takes to hop to another site or cell. For a one-dimensional system one generally finds two adsorption sites, on-top and bridge, per unit cell. For a hexagonal lattice we have one on-top, three bridge and two hollow sites per unit cell. Such systems can be represented by an n-site lattice gas model where $n = 2$ or 6 for a linear and a hexagonal lattice, respectively. A further assumption in identifying adsorption sites is, of course, that the adsorbate forms commensurate structures with the surface lattice. In molecular adsorption the adparticle might have several preferred orientations in a given adsorption site in which case we allow each site to have several adsorption states. For CO on Pt(1 1 1) this does not seem to be the case, at least for coverages not exceeding 1/2 ML.

To set up the lattice gas model for an adsorbate on a hexagonal lattice we label the unit cells of the lattice by an index $i = 1, \ldots, N_s$ and introduce occupation numbers $t_i = 0$ or 1 depending on whether the top site in unit cell i is empty or occupied; similarly for the three bridge sites $b_i^{(j)}$, $j = 1, 2, 3$, and two hollow sites $h_i^{(j)}$, $j = 1, 2$. Because different sites in the same cell cannot be occupied simultaneously we also have exclusion conditions like $t_i b_i^{(j)} = 0$. Also, we can safely assume hardcore exclusions between CO molecules on sites in neighboring cells that are separated by less than a lattice constant. For what follows we neglect hollow sites because their contribution is not observed for CO on Pt(1 1 1) below 1/2 ML. A

microstate of such an adsorbate with N_s sites is then specified by a vector with $4N_s$ components

$$(\mathbf{t}, \mathbf{b}^{(1)}, \mathbf{b}^{(2)}, \mathbf{b}^{(3)}) = \left(t_1, b_1^{(1)}, b_1^{(2)}, b_1^{(3)}; t_2, b_2^{(1)}, b_2^{(2)}, b_2^{(3)}, \dots\right) \quad (1)$$

The Hamiltonian of the system reads

$$H(\mathbf{t}, \mathbf{b}) = \sum_i \left(E_t t_i + E_b \sum_{j=1}^{3} b_i^{(j)}\right) + \frac{1}{2} \sum_n \sum_i \sum_{a_n=1}^{C_n} \left[V_n^{(tt)} t_i t_{i+a_n} + \sum_{j=1}^{3} \left(V_n^{(tb)} t_i b_{i+a_n}^{(j)} + \sum_{j'=1}^{3} V_n^{(bb)} b_i^{(j)} b_{i+a_n}^{(j')}\right)\right] \quad (2)$$

Here the sum on i exhausts all lattice cells and a_n enumerates the nth neighbors, with coordination C_n, surrounding a site t_i or b_i. E_t and E_b are the free energies of a single molecule adsorbed in the on-top and bridge site, respectively, given (here for the on-top site, with a similar expression for the bridge sites) by

$$E_t = E_t(T) = -V_0^{(t)} - k_B T \ell n\left(q_3^{(t)} q_{int}^{(t)}\right) \quad (3)$$

where $V_0^{(t)}$ is the (positive) binding energy of an isolated molecule on the surface. Moreover,

$$q_3^{(t)} = q_z^{(t)} q_{xy}^{(t)} \quad (4)$$

is the vibrational partition function of an adsorbed particle for its center of mass vibrations with respect to the surface, with

$$q_z^{(t)} = \exp\left(h\nu_z^{(t)}/2k_B T\right) / \left[\exp\left(h\nu_z^{(t)}/k_B T\right) - 1\right] \quad (5)$$

its component for the motion perpendicular to the surface. Likewise, $q_{xy}^{(t)}$ is the partition function for the motion parallel to the surface. We have also allowed for the fact that the internal partition function for rotations and vibrations of an adsorbed molecule is changed from its free gas phase value, Z_{int} to $q_{int}^{(t)}$, if some of the internal degrees of freedom are frozen out or frustrated. For the gas phase we have

$$Z_{int} = Z_{vib} Z_{rot} \quad (6)$$

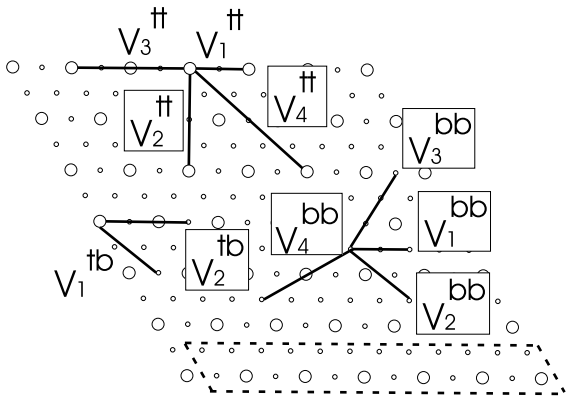

Fig. 1. Schematic of on-top (large circles) and bridge (small) binding sites on Pt(1 1 1). Solid lines indicate some of the CO–CO interactions in the lattice gas Hamiltonian. The strip of sites bounded by the dashed line is used in the construction of the transfer matrix.

where Z_{vib} has the form of (5) with an effective vibrational temperature, T_{vib}, for the internal stretch; Z_{rot} is well expressed in terms of the gas phase rotational temperature, T_{rot}, by T/T_{rot} for heteronuclear CO. For $q_{int}^{(t)}$ we assume a product of 1-d oscillator expressions (5)—one stretch and two orthogonal frustrated rotations—with frequencies $\nu_v^{(t)}$, $\nu_{r_1}^{(t)}$, $\nu_{r_2}^{(t)}$, respectively.

The square-bracketed terms in (2) account for lateral interactions between adsorbed molecules in pairs of unit cells, e.g. $V_1^{(tt)}$, $V_1^{(bb)}$ and $V_1^{(tb)}$ are interactions between first neighbor cells; $V_1^{(tb)}$ is of longer range, however. The designation of some first, second and third neighbors is illustrated in Fig. 1.

3. Equilibrium

3.1. Preliminaries

To calculate the equilibrium properties of the adsorbate we evaluate the grand partition function ($\beta = 1/k_B T$)

$$\Xi(T, N_s, \mu_t, \mu_b) = \sum_{\mathbf{t},\mathbf{b}} \exp\left[-\beta\left(H(\mathbf{t}, \mathbf{b}) - \mu_t \Sigma_i t_i - \mu_b \Sigma_i (b_i^{(1)} + b_i^{(2)} + b_i^{(3)})\right)\right] \quad (7)$$

from which we get the grand potential

$$\Omega(T, N_s, \mu_t, \mu_b) = -k_B T \ln \Xi \tag{8}$$

Derivatives with respect to the chemical potentials give the partial on-top and bridge coverages

$$\begin{aligned} \theta_t &= \left.\frac{\partial \Omega}{\partial \beta \mu_t}\right|_{T,N_s} = N_s^{-1} \sum_i \langle t_i \rangle \\ \theta_b &= \left.\frac{\partial \Omega}{\partial \beta \mu_b}\right|_{T,N_s} = N_s^{-1} \sum_{i,j} \langle b_i^{(j)} \rangle \end{aligned} \tag{9}$$

Then we equate the chemical potentials, $\mu_t = \mu_b = \mu_{ad}$, to find $\theta = \theta_t + \theta_b = \theta(T, \mu_{ad})$ or, upon inversion, $\mu_{ad}(T, \theta)$. In equilibrium with the (ideal) gas phase above the surface at pressure P, the adsorbate and gas phase chemical potentials are equal $\mu_{ad} = \mu_{gas}$, where

$$\exp[\beta \mu_{gas}] = \frac{P}{k_B T} \lambda_{th}^3 \frac{1}{Z_{int}} \tag{10}$$

Here $\lambda_{th} = h/\sqrt{2\pi m k_B T}$ is the thermal deBroglie wavelength. From the resulting isobars or isotherms, $\theta = \theta(T, P)$, we can calculate the isosteric heat of adsorption

$$Q_{iso}(\theta, T) = -\left.\frac{\partial(\ln P)}{\partial \beta}\right|_{\theta} \tag{11}$$

The grand canonical partition function is calculated using either the transfer matrix or Monte Carlo methods. The transfer matrix is constructed by standard methods [35] for interactions between adparticles in a pair of adjacent rows of the hexagonal lattice, each consisting of N_s top sites and the neighboring $3N_s$ bridge sites with periodicity imposed at row ends e.g. periods 2,3 for a minimum $N_s = 6$. (Such a row is outlined in Fig. 1.) The states (occupancies) of each of the $4N_s$ sites are generated with regard to site exclusions; symmetries—rotations, and reflections of the row—reduce the number of independent states, the matrix dimension, to, e.g. 374 for $N_s = 6$. Boltzmann weights are evaluated in this basis for finite interactions for all top/bridge combinations within the row. Similarly, weights are constructed for interactions between particles in adjacent rows. The grand partition function follows from the leading eigenvalue, λ_1, of this matrix, $\Xi = \lambda_1^{N_s}$. In practice, only the symmetric subblock of the matrix is required for the calculation of the total coverage, $\theta(\mu_{ad}, T)$, which is obtained from the leading eigenvector, as are the partial coverages of the two adsorption sites and particle–particle correlations. With $N_s = 6$ this row–row transfer matrix suffices for essentially 'exact' equilibrium quantities for most interactions between neighbouring unit cells.

The advantages of the transfer matrix method are its numerical accuracy and computational efficiency. However, the dimension of the transfer matrix becomes too large when long-ranged lateral interactions need to be included. We have therefore used Monte Carlo methods for such calculations. Simulations were performed in both the grand canonical and canonical ensembles (chemical potential and coverage specified, respectively) using the Metropolis algorithm (with spin flip and infinite Kawasaki dynamics, respectively) [36]. Equilibration times of the order of 2^{17} Monte Carlo sweeps were allowed for each coverage or chemical potential point. The system was initialized with top sites only in the canonical ensemble and with a bare substrate in the grand-canonical ensemble for the first temperature-coverage, temperature-chemical potential point, respectively. Thereafter, to hasten equilibration, initialization of the system occurred with the final configuration of the previously calculated point. For temperatures below 350 K we performed an average over at least three independent samples. The resulting relative error of $\theta(\mu, T)$, for example, was as small as 10^{-3}. For lowest temperatures and coverages where metastable ordering of the adsorbate could occur, e.g. around 1/2 ML, we averaged over as many as twenty samples, for an error around 1 part in 50. To allow adsorption on bridge and top sites we used four interpenetrating 48×48 lattices, with periodic boundary conditions. This lattice size was chosen to allow commensurate low-coverage ordered structures with periods of 3, 4 or 8.

Within the framework of the multi-site lattice gas model a comprehensive analysis of the available data amounts to finding a set of energetic and vibrational parameters in the Hamiltonian that fits all the data. The ideal approach to this would be to perform ab initio calculations based on density functional theory, for instance, as has been done

recently for the O/Ru(0 0 0 1) system [37]. Unfortunately, density functional calculations for CO/Pt(1 1 1) have persistently given a preference for hollow over top-site adsorption at vanishing coverage, in contradiction to experimental evidence [33]. A recent relativistic DFT calculation [34] produces the correct binding order but, as we shall see, gives incorrect binding energies, most likely attributable to the cluster size and geometry which does not sufficiently represent the bonding environment on a (1 1 1) surface. Also, there are no calculations available for small to medium coverages from which one could extract the lateral interactions, as was done for the O/Ru(0 0 0 1) system. Such calculations have to await significant improvements in the accuracy of DFT methods because, unfortunately, the energy differences and interactions are typically of the order of a few k_BT in the desorption range, i.e., a fraction of the total energy of the relatively large units cells at small coverages. Therefore we resort to a phenomenological procedure to determine the parameters in the Hamiltonian, a procedure that has worked well for other systems. This is done by fitting and analyzing selected sets of quality experimental data. Although uniqueness of the parameter set cannot be guaranteed in such an approach it is highly plausible if and when we can explain a larger and varied set of data.

3.2. Equilibrium at low coverage

We begin our analysis with the observation that, at the lowest coverages, both lateral interactions between CO molecules as well as the more weakly binding bridge sites must play a negligible role. This allows us to determine the parameters in E_t, given in (3), namely the on-top site binding energy and the vibrational frequencies. The latter are measured in IR, EELS and helium scattering experiments and are listed in Table 1.

The top-site binding energy is best determined by fitting the low coverage region of pressure isotherms [18]. To describe this limit properly we first express the adsorbate chemical potential as the sum of the top-site free energy, a term describing a non-interacting lattice gas, and the remaining coverage and temperature dependence which incorporates the site binding difference and all lateral interactions, $\mu_{\rm lat}(\theta,T)$,

$$\mu_{\rm ad}(\theta,T) = -V_0^{(t)} + k_BT\Big[\ln(\theta/(1-\theta)) - \ln\left(q_3^{(t)}q_{\rm int}^{(t)}\right)\Big] + \mu_{\rm lat} \tag{12}$$

The pressure is then given by

$$P(\theta,T) = \frac{\theta}{1-\theta}\frac{1}{\lambda_{\rm th}^3}\frac{k_BT}{h}\frac{Z_{\rm int}}{q_3^{(t)}q_{\rm int}^{(t)}}\,e^{-V_0^{(t)}/k_BT}e^{\mu_{\rm lat}/k_BT} \tag{13}$$

At lowest coverages, where interactions are irrelevant, we can set $\mu_{\rm lat}$ to zero and derive the low-coverage heat of adsorption,

$$Q_{\rm iso}(\theta=0,T) = V_0^{(t)} - \frac{d}{d\beta}\ln\left[\frac{Z_{\rm int}}{q_3^{(t)}q_{\rm int}^{(t)}}\right] + (5/2)k_BT \tag{14}$$

The experimental value of $Q_{\rm iso}(0,T)$, in the temperature range 400–450 K, follows from an analysis of the pressure data of Poelsema et al. [18]. We find $Q_{\rm iso}^{(\rm exp)} = 142 \pm 7$ kJ/mol. This gives $V_0^{(t)} \simeq 149$ kJ/mol and a contribution to $Q_{\rm iso}$ from the gas- and adsorbed-phase vibrational and rotational modes of about 9/2 k_BT, in magnitude. Anticipating later results we can state that these parameters also reproduce the high-temperature/low-coverage TPD traces. Note that $Q_{\rm iso}(0,T)$ and $V_0^{(t)}$ are both distinct from the "activation energy of desorption" defined by Poelsema et al.

Table 1
Site translational and internal vibrational modes of CO on Pt(1 1 1), in units of Kelvin [14]

$h\nu/k_B$	ν_x	ν_y	ν_z	ν_v	ν_{r1}	ν_{r2}
top	70	70	690	3024	592	592
bridge	86	207	547	2664	518	772

CO gas phase values are $T_{\rm rot} = 2.77$ K, $T_{\rm vib} = 3103$ K [1 cm^{-1} = 1.44 K; 1 meV = 8.06 cm^{-1}].

3.3. Equilibrium partial coverages

To determine the binding energy of bridge sites, and other parameters, we turn to the results of time resolved EELS and XPS experiments, from which the site partial coverages, θ_t, θ_b, have been determined as functions of instantaneous coverage. The results of Kinne et al. [20], for both isothermal adsorption and temperature-programmed experiments, imply that these partial coverages assume their equilibrium values for all temperatures above 100 K, or so. This conclusion is in agreement with Mieher et al. [9] who observed reversible population of bridge and top sites for total coverages below 0.5 ML and temperatures ramped between 95 K to just below desorption temperatures. However, it disagrees with Cudok et al. [15]; they found a flux dependence of partial coverage evolution between 100 and 300 K. The origin of this discrepancy is unclear. As the recent diffusion measurements of Nekrylova and Harrison [30] support the assumption of equilibrium in the adsorption temperature range, we shall use Kinne's data as the primary set to be fitted.

The main features of these partial coverage vs. coverage plots are (cf. Fig. 5 of [20] and Fig. 3 below): At lowest temperatures ($\gtrsim 100$ K) the on-top CO coverage, θ_t, rises linearly with θ, to about 0.2 ML, before significant bridge coverage, θ_b, occurs. Then θ_b rises to match θ_t at 0.5 ML, $\theta_t \simeq \theta_b \simeq 0.25$ ML; above 0.5 ML both partial coverages increase together with $\theta_t \lesssim \theta_b$, i.e. a (temporary) crossover of partial coverages is apparent. For $T \simeq 200$ K, the onset of the bridge population starts at lower total coverage. Again, $\theta_t \simeq \theta_b$ at 0.5 ML but the partial coverages now diverge above this point, with θ_b decreasing. For highest adsorption temperatures ($T = T_{ha} \lesssim 300$ K) the bridge population is first discernible around $\theta = 0.1$ ML, and θ_t and θ_b are strictly increasing with θ with $\theta_b < \theta_t$ at 1/2 ML.

These relative occupations of top and bridge sites can be simply understood by considering the effects of (i) the binding energy difference, $\Delta V_0 = V_0^{(t)} - V_0^{(b)}$ and (ii) significant repulsions for CO adsorbed on both neighboring top sites and bridge sites. The latter condition implies nearest neighbor site exclusion which results in equal occupancy of top and bridge sites at 1/2 ML. A straightforward demonstration of these effects is given in Appendix A for a one-dimensional system. The existence of any $(\sqrt{3} \times \sqrt{3})R30°$ structure confirms that the first neighbour interaction, $V_1^{(tt)}$, is important (as it is on almost all metal surfaces). Also, the $c(4 \times 2)$ structure formed at 1/2 ML will only occur if the bridge–bridge CO interaction, $V_1^{(bb)}$, is comparable. Thus the essential behaviour of the partial coverage curves should be determined by these three energies. If all three are much larger than $k_B T_{ha}$, then the maximum coverage is restricted to 1/2 ML, the partial coverage of top sites, θ_t, will rise linearly with total coverage to a maximum of 1/3 ML, at which point the bridge site occupation will start, rising linearly, with θ_t decreasing concurrently. Experimentally only a diffuse $(\sqrt{3} \times \sqrt{3})R30°$ structure is observed around 150 K but not at higher temperatures. On the other hand, at all temperatures (above 100 K) θ_t is nearly monotonic implying that these energies are closer to a few $k_B T_{ha}$. This is confirmed simply for ΔV_0 by the temperature dependence of the bridge partial coverage, at its onset, in the range 100–300 K. An illustrative calculation is shown in Fig. 2: the piecewise linear behaviour of θ_t, θ_b, and the peak in θ_t at 1/3 ML, at low temperature (150 K) disappears at higher temperature (275 K). We can suppress this peak for all temperatures by including a longer-ranged interaction, such as a weak second neighbor repulsion on top sites, $V_2^{(tt)} < k_B T$. Although this additional on-top CO repulsion now causes the partial coverages to cross below 1/2 ML—which is not observed—we have the qualitative features of the partial coverages, in the experimental temperature range, with these energy scales.

For a quantitative fit of the partial coverages we have to stabilize the $c(4 \times 2)$ structure at 1/2 ML and ensure that the bridge occupation remains at or below that of top sites above 1/2 ML. Also, we must produce an observed temperature dependent partial-coverage gap at 1/2 ML, starting at about 250 K. The stabilization occurs with a weak attraction between the neighbouring top and bridge-site CO, $V_1^{(tb)} < k_B T$, forming the $c(4 \times 2)$ phase; longer-ranged bridge interactions, $V_n^{(bb)}$, $n = 2$–5, fix $\theta_b < \theta_t$ and above 1/2 ML. Finally, we need a

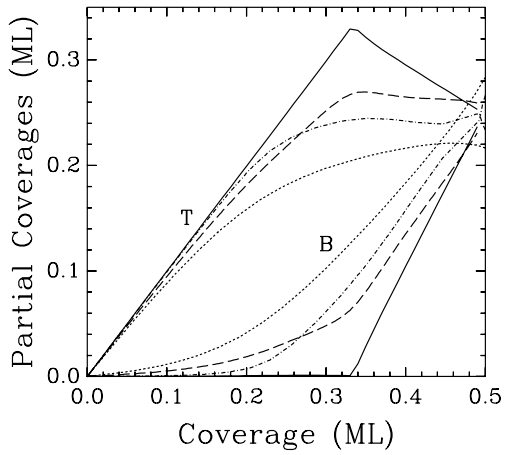

Fig. 2. Top (T) and bridge (B) site coverages, as a function of total coverage, for representative binding energy differences and a minimal number of interactions. Upper four curves: top-sites with (top to bottom at 1/3 ML) $\Delta V_0/k_B = 1200$ K, $V_1^{(tt)}/k_B = 1100$ K, $V_1^{(bb)}/k_B = 1000$ K for $T = 150$ K (solid line) and 275 K (dashed); $\Delta V_0/k_B = 1000$ K, $V_1^{(tt)}$, $V_1^{(bb)}$ unchanged, $V_2^{(tt)}/k_B = 70$ K for $T = 150$ K (dash-dotted) and 275 K (dotted). Corresponding bridge coverages below.

small third neighbour top interaction, $V_3^{(tt)}$, and some adjustments of the major energy scales to achieve a good fit to the partial coverage data, (Fig. 3). Our interactions are listed as Set 1 in Table 2. Significantly, interactions beyond $V_1^{(tt)}$ and $V_1^{(bb)}$ are less than k_BT at the lowest temperature (100 K). In adjusting these secondary interactions we have also been guided by corresponding features of the experimental partial coverages above 1/2 ML, such as their slopes and the crossings at low temperature. However, we have not attempted to extend our results to 0.6–0.66 ML and to reproduce the compressed structures observed there. Reproduction around 1/2 ML is affected further by the temperature-dependent part of the site binding difference, E_b-E_t, which can be approximated by a value of about $1.2(T - 150)k_B$ for the frequencies in Table 1, i.e. it varies by about 200 k_B for the temperature span of Fig. 3.

An examination of site correlations confirms that, up to about 150 K, the first significant though weakly ordered structure is the $(\sqrt{3} \times \sqrt{3})R30°$ pattern. As coverage grows beyond 1/3 ML this diminishes and is replaced by the $c(4 \times 2)$ pattern. The latter persists to about 275 K. These features are in accord with experiment.

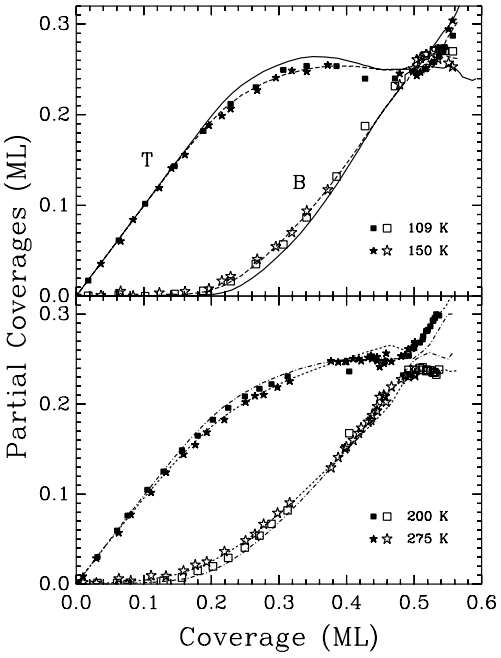

Fig. 3. Experimental partial coverages as a function of CO coverage for top (T) and bridge (B) sites (full and open symbols, respectively) at four substrate temperatures and a CO pressure of 4×10^{-8} mbar. The corresponding theoretical curves, calculated with the parameters of Tables 1 and 2, Set 1, are the solid ($T = 109$ K), dashed (150 K), dash-dotted (200 K) and dotted (275 K) lines, respectively.

Table 2
Interaction energies in the lattice gas model, in units of Kelvin for ease of comparison with adsorption and desorption temperatures

	ΔV_0	$V_1^{(tt)}$	$V_2^{(tt)}$	$V_3^{(tt)}$	$V_4^{(tt)}$	$V_1^{(bb)}$	$V_2^{(bb)}$	$V_3^{(bb)}$	$V_4^{(bb)}$	$V_1^{(tb)}$	$V_2^{(tb)}$
Set 1	1200	1100	95	45	0	1000	125	85	25	−50	0
Set 2	1100	1390	310	230	30	985	435	320	260	290	260

Interactions for Set 2 extend beyond those indicated, to tenth neighbor on bridge sites ($V_{10}^{(bb)}$) and sixth neighbor for top and bridge sites ($V_6^{(tb)}$). Their values decrease with range, d, as d^{-3}, roughly. Where indicated in the text Set 1 is augmented by a mean field interaction V_{mf}.

Our results, when compared to the DFT calculations [34], indicate a primary hurdle for the acceptance of ab initio methods for this system (see also our criticisms at the end of Section 3.1): Geschke et al. calculate an on-top binding energy of $V_0^{(t)} = 2.30$ eV and a binding difference to bridge sites of $\Delta V_0 = 430$ meV; from our fits to data we estimate 1.54 ± 0.07 eV and 95 ± 15 meV, respectively. The magnitudes of our fitted secondary interactions, below 10 meV, are in the noise of present DFT calculations.

3.4. Pressure isotherms and heat of adsorption

With all energies in the Hamiltonian determined we can now calculate all other equilibrium properties, in particular the pressure isotherms at finite coverage [18] and the resulting isosteric heat of adsorption. As we can see from Fig. 4(a), dashed lines, the fit to the pressure data is poor—illustrating the fact that a model that reproduces one set of data can still be insufficient and not capture all the physics of the system. The calculated isotherms are too steep implying that the overall repulsion in our model is too small. This is not surprising because the CO–CO repulsion is dipolar-like and therefore long ranged and we have so far only included significant repulsions to first neighbor. This is corroborated by an analysis of the data which shows that the heat of adsorption decreases linearly with coverage which, in turn, implies a linear rise of the chemical potential with coverage, and more rapidly than our calculated values. This is typical mean field behavior for long-ranged dipolar interactions. The simplest way to account for this is to add a mean field term, $V_{\mathrm{mf}}\theta$, to the Hamiltonian and adjust its strength to obtain a satisfactory fit to the pressure isotherms, solid lines in Fig. 4(a). This yields $V_{\mathrm{mf}} = 40 \pm 5$ kJ/mol/ML. To illustrate the relative contributions to the chemical potential we plot $\mu_{\mathrm{lat}}(\theta, T)$ in Fig. 4(b) for a range of temperatures but for $V_{\mathrm{mf}} = 0$. (By its definition in (12) μ_{lat} may decrease with increasing coverage, unlike μ_{ad}.) Noteworthy is that μ_{lat} is approximately linear in θ to about 1/4 ML and not strongly temperature dependent for the temperatures of Fig. 4(a), i.e. the primary energy parameters ΔV_0, $V_1^{(\mathrm{tt})}$, $V_1^{(\mathrm{bb})}$, already produce a mean field-type behaviour. The straight line (index 2), is the additional energy, $V_{\mathrm{mf}}\theta$, we must add to this μ_{lat} to fit the pressure isotherms—30–40% larger than the contribution of short-ranged interactions. We calculate the isosteric heat of adsorption using the total chemical potential but in two temperature regimes. In the desorption temperature range ($T \gtrsim 300$ K), μ_{lat} is unstructured and Q_{iso}, averaged over such temperatures, decreases with coverage almost linearly to 1/2 ML, Fig. 4(c), lower dotted line. Not surprisingly, its initial slope is just that determined by Poelsema et al. (68.5 kJ/mol/ML) by their analysis of their low-coverage isotherms. In the adsorption temperature range ($T \lesssim 275$ K), μ_{lat} has structure, particularly around 1/2 ML and the temperature average of Q_{iso} differs (upper dotted line). Here the rise in Q_{iso} below 1/2 ML signals the $c(4 \times 2)$ ordering; it derives from the inflections of μ_{ad} for these coverages—where μ_{lat} dips in Fig. 4(b)—and has been discussed elsewhere [38]. (Similar features have been observed for CO/Ru(0 0 0 1) but at the onset of the $(\sqrt{3} \times \sqrt{3})R30°$ ordering [39,40].) The subsequent sudden drop of Q_{iso} occurs because CO is now forced to occupy first neighbor cells. These two curves in Fig. 4(c) illustrate that measured values of Q_{iso} depend on the temperature and coverage ranges examined.

It is not necessary to summarily account for the long-ranged interactions with a mean field. Instead, we can add further interactions, out to the third unit cell in our case (limited by computer capacity), and choose their strength to decay roughly according to a dipolar repulsion, for example, inversely proportional to the third power of the distance. Again, these interactions are to be determined by fitting the partial coverages for all temperatures, as well as the pressure data. In this we succeed well (see Fig. 5), except at the lowest temperature. At 109 K the $(\sqrt{3} \times \sqrt{3})R30°$ structure at 1/3 ML is apparent in the partial coverage as is another structure 0.08 ML above. Particle correlators indicate that the latter is an artifact of our truncation of the interactions beyond a range of $\sqrt{7}$ times the lattice constant. However, at high temperature these interactions give essentially the same pressure isotherms as the mean field treatment, i.e. a similar chemical potential. These interactions appear as Set 2 in Table 2.

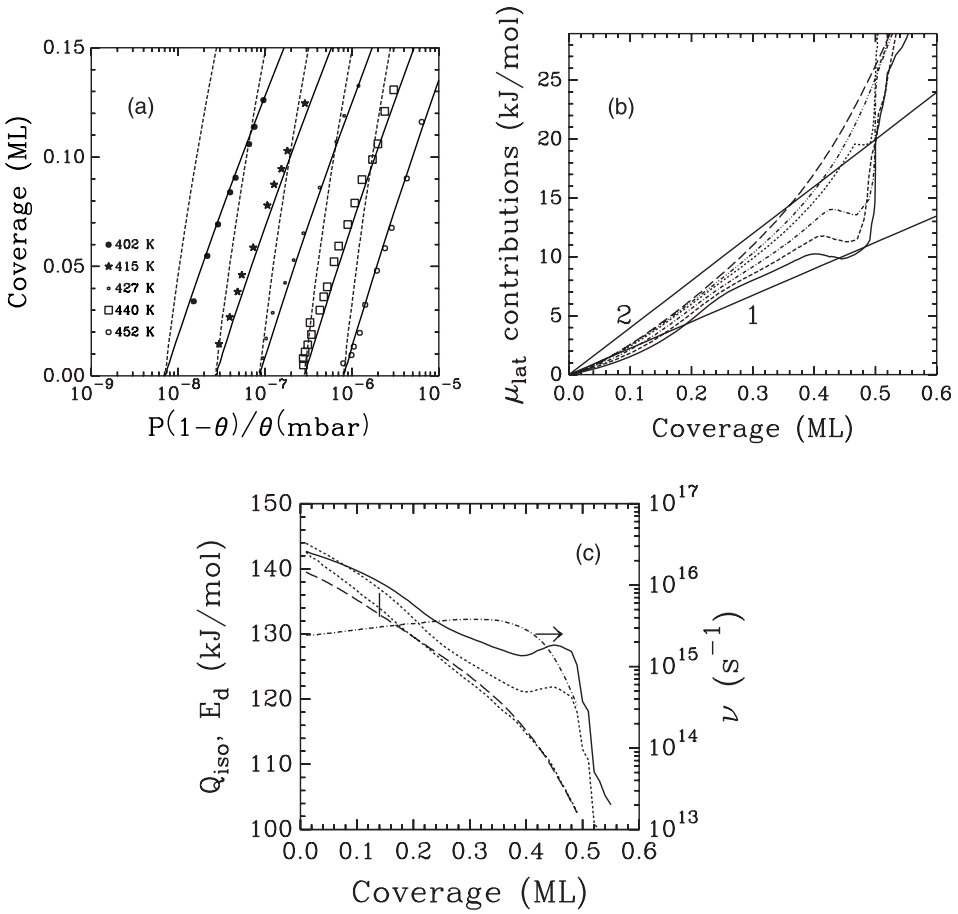

Fig. 4. (a) CO coverage, θ, as a function of the scaled pressure for several adsorption temperatures. Data (symbols) from [18]. Dashed lines: theoretical curves for $V_0^{(t)} = 150.2$ kJ/mol, site frequencies of Table 1, site-binding difference and interactions of Set 1, Table 2. Solid lines: theory with a mean field CO interaction of $V_{mf} = 40$ kJ/mol/ML, in addition. (b) Contributions to the adsorbate chemical potential: μ_{lat}, calculated for the parameters of Tables 1 and 2 (Set 1), as a function of coverage and temperatures (bottom to top at 0.4 ML) 109, 150, 200, 275, 330, 450 K. Straight lines: mean-field contributions for $V_{mf} = 22.5$ and 40 kJ/mol/ML, lines 1, 2 respectively. (c) The temperature-averaged isosteric heat of adsorption, Q_{iso}, as function of coverage, calculated for three schemes. Solid line: $V_0^{(t)} = 148.8$ kJ/mol, parameters of Fig. 4(b) with $V_{mf} = 22.5$ kJ/mol/ML, low-temperature average ($T < 275$ K). Dotted lines: $V_0^{(t)} = 150.2$ kJ/mol, parameters of Fig. 4(b) with $V_{mf} = 40$ kJ/mol/ML, low-temperature average (upper dotted curve); and high-temperature average, over isotherms of Fig. 4(a) (lower dotted curve). The vertical bar indicates the coverage limit of that data. Dashed line: average desorption energy, $E_d(\theta)$, obtained from an Arrhenius analysis (heating-rate variations) of model TPD data such as in Fig. 10(b). Dash-dotted line: corresponding exponential prefactor $\nu(\theta)$ (right-hand ordinate).

Although our calculated chemical potential permits a very good fit to the isotherms, we alert the reader that it is incapable of reproducing TPD spectra. In particular, about half the value of V_{mf} is necessary to fit the TPD spectra and still allow a reasonable fit to the isotherms within the experimental uncertainties, as we will discuss in Section 5.

4. Adsorption kinetics

4.1. Preliminaries

In this section we use the kinetic lattice gas model to calculate the adsorption kinetics and the sticking coefficients, in particular. Some clarifying comments are in order.

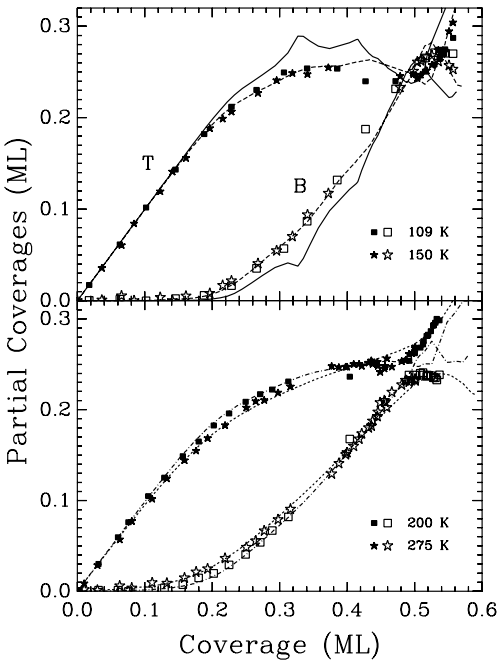

Fig. 5. Description as Fig. 3 but calculated with Set 2 of Table 2.

Assuming that the individual microscopic events of adsorption, desorption and diffusion can be modeled as Markovian processes one can show rigorously, on the basis of the kinetic lattice gas model [35], that the macroscopic equations for the time evolution of the two-site adsorbate are given by

$$\frac{d\theta_t}{dt} = S_t \frac{Pa_s\lambda_{th}}{h} + \left.\frac{d\theta_t}{dt}\right|_{des} + \left.\frac{d\theta_t}{dt}\right|_{diff(t-t)} + \left.\frac{d\theta_t}{dt}\right|_{conv} \tag{15}$$

$$\frac{d\theta_b}{dt} = S_b \frac{Pa_s\lambda_{th}}{h} + \left.\frac{d\theta_b}{dt}\right|_{des} + \left.\frac{d\theta_b}{dt}\right|_{diff(b-b)} - \left.\frac{d\theta_t}{dt}\right|_{conv} \tag{16}$$

The adsorption term is the flux of incoming particles times a sticking coefficient. The desorption term will be discussed in the next section. The diffusion terms account for site-to-site hopping and interconversion between top and bridge sites. If the rate of hopping is large compared to the rate of adsorption and desorption the adsorbate will be maintained in quasi-equilibrium throughout its macroscopic evolution implying that the partial coverages and all particle correlations depend only on the instantaneous total coverage, $\theta(t)$, and temperature. This is the case in the temperature range of desorption, with few exceptions, but not at the lowest temperatures of adsorption where non-equilibrium effects come into play. In this case the sticking coefficients are functions of the local environment of a particular adsorption site and the full formalism of the kinetic lattice gas model is needed to determine the evolution.

For CO/Pt(1 1 1) there is good evidence that at temperatures as low as 100 K diffusion is faster than adsorption. Kinne et al. have not detected any dependence of the partial coverages as a function of time on the flux of the incoming beam for two decades of pressure below 10^{-7} Torr at 109 K. This is also confirmed by the diffusion measurements which indicate that the top-bridge conversion rates are some 20–200 times faster than adsorption rates for these pressures and temperatures [29,30].

In the presence of top-bridge site conversion the time evolution of the partial coverages in an adsorption experiment, i.e. under conditions where desorption is negligible, will be the result of both adsorption into a top or bridge site (controlled by the same flux but different site sticking coefficients) and site conversion. Thus no information about site sticking, S_t and S_b, can be extracted from such measurements directly. On the other hand the total sticking coefficient, $S = (S_t + 3S_b)/4$, is given directly by the slope of the total coverage vs. exposure curves; the numerical factors arise from the fact that incoming particles are equally likely to adsorb in one top and three bridge sites.

To calculate these sticking coefficients we resort to the kinetic lattice gas model and follow the general theory given earlier [41], and more recently applied to a 1-d system with two adsorption sites [42], and calculate the sticking for both direct (chemisorption) and indirect (precursor-mediated) processes. It is known that the sticking coefficient of CO on metal surfaces is more or less coverage independent in the low to medium coverage region, indicating that sticking is precursor-mediated. We will show presently that direct sticking does not show such a behavior but decreases

steadily. We shall see the various effects of strong repulsions and site exclusion corroborating the ideas we advanced previously for 1-d systems. An understanding of direct sticking is also useful because of the similarity of its coverage dependence to that of the conversion from the precursors to the chemisorption state.

4.2. Direct sticking

Sticking into a top site, for example, is only possible if the surrounding six bridge sites are also vacant. Further neighbors influence the sticking probability according to

$$S_t(\theta,T) = S_0(T)\left\langle (1-t_0)\prod_{j=1}^{6}(1-\tilde{b}_0^{(j)})\left[1 + A_1^{(tt)}\sum_{j=1}^{6} t_j + A_2^{(tt)}\sum_{j\neq j'=1}^{6} t_j t_{j'} + \cdots\right]\right\rangle \quad (17)$$

for sticking into a central top site with occupation number t_0. Here $\tilde{b}_0^{(j)}$ denotes the occupation numbers of the six surrounding bridge sites, and $t_{j\neq 0}$ refers to the first neighbor top sites. The terms in the square brackets extend to summations over all six neighboring top sites and also to further bridge and top sites, as defined by the Hamiltonian. This is a generalization of the scheme presented in detail elsewhere [41,42] where explicit expressions for the coefficients can also be found. All correlators in (17) are calculated for the system in equilibrium and so account for all lateral interactions. Because our system has very large first neighbor repulsions, $V_1^{(tt)}$, $V_1^{(bb)} \gg k_B T$, at least for adsorption temperatures below 200 K, the coefficients $A_n^{(aa)}(a = t, b; n = 1\text{–}6)$ dominate and we are left with sticking into a hard-core environment, consisting of a hexagon of excluded first neighbors of the same site type in addition to excluded top or bridge sites bounded by this hexagon; for top sites we get

$$S_t(\theta,T) = S_0(T)\left\langle (1-t_0)\prod_{j=1}^{6}(1-\tilde{b}_0^{(j)})(1-t_j)(1-\tilde{b}_j^{(j)})\right\rangle \quad (18)$$

This, and a similar expression for bridge sites, is the primary result which allows for an understanding of the adsorption kinetics of CO/Pt(1 1 1).

To put the effect, on the sticking, of infinite first neighbour repulsion on an hexagonal lattice into perspective, we first mention the case of a lattice with one adsorption site, labelled t. In this case the maximum coverage is 1/3 ML. This is the hard hexagon model for which the equilibrium statistical mechanics has been solved exactly [43]. The sticking coefficient is given exactly by (18) with $\tilde{b}_k^{(j)} = 0$. Alternately, we can use adsorption–desorption equilibrium and rewrite this as

$$S(\theta,T) = S_0(T)\theta\exp[\beta(E_t - \mu_{ad}(\theta,T))] \quad (19)$$

and thus more easily determine its coverage dependence by calculating the chemical potential of the adsorbate, in the limit of vanishing temperature. We can also apply the factorization scheme for correlators developed previously for a 1-d system to (18) to yield an analytic form, in lowest approximation given by

$$S(\theta,T) = S_0(T)\frac{(1-3\theta)^5}{(1-2\theta)^4} \quad (20)$$

This result agrees with the exact result for all coverages, within a few per cent, except above 0.27 ML, where the hard hexagon system undergoes an order–disorder transition. However, the exact value is small here already (<0.03). Both forms start out as $(1-7\theta)$, because of site exclusion, and both vanish at 1/3 ML.

The presence of a second binding site implies that, above a coverage of 1/3 ML, CO can spill over already from the top sites to avoid the (infinite) nearest neighbor repulsion. This keeps the sticking coefficient non-zero up to a coverage of 1/2 ML (and higher if the nearest neighbor repulsions are not taken to be infinite). In Fig. 6 we show the direct sticking, for both top and bridge sites, obtained with all correlators calculated for the interactions of Set 1 in Table 2 included on the right hand side of (17), and for temperatures at the top end of the adsorption and desorption ranges. We also show the hardcore sticking for each site (dashed lines). At low temperature this follows the direct sticking closely until, around 1/3 ML, the

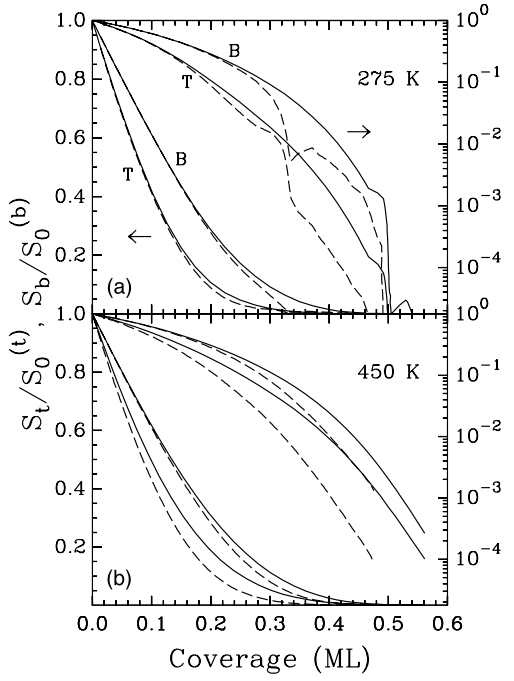

Fig. 6. Coverage dependence of the direct on-top and bridge site-sticking coefficients, linear and logarithmic scales, for two interaction parameter sets and two temperatures. Solid lines: parameters of Tables 1 and 2 (Set 1). Dashed lines: same site binding difference but $V_1^{(tt)}$, $V_1^{(bb)}$ both infinitely repulsive (hard core sticking). Panels: (a) $T = 275$ K, (b) $T = 450$ K.

first neighbor exclusions on both sites make their presence felt, with a characteristic sharp drop of the hardcore-sticking into top sites and a minimum of the sticking coefficient for bridge sites as ordering occurs [42]. Interactions beyond first neighbors have little influence on direct sticking below 1/2 ML, although they are not inconsequential above this point. For low coverage the direct sticking coefficients decrease linearly according to

$$S_t \simeq S_0^{(t)}(1 - 7\theta_t - 4\theta_b) \tag{21}$$

$$S_b \simeq S_0^{(b)}(1 - 4\theta_t - 5\theta_b) \tag{22}$$

Top site sticking decreases faster because of the preferential binding to these sites, in other words, because there are relatively more empty bridge sites, due to their smaller binding energy, the probability of sticking into these sites is greater.

4.3. Precursor-mediated sticking

As we indicated above direct sticking bears no resemblance to the experimental situation for CO on metals. Therefore we turn to precursor-mediated sticking.

When conversion from extrinsic to intrinsic precursors is fast, the conversion from the precursor to the final chemisorbed state occurs mainly from the intrinsic precursor. The net sticking coefficient then reads [41], again given here only for sticking into the top sites,

$$S_t^{(\mathrm{prec})}(\theta,T) = \left(S_0^{(i)}(1-\theta) + S_0^{(e)}\theta\right) \times \frac{r_{c\leftarrow i}^{(t)}(\theta,T)(1-\theta)}{\left(r_{c\leftarrow i}^{(t)}(\theta,T) + r_i(T)\right)(1-\theta) + r_e(T)\theta} \tag{23}$$

Assuming that sticking into and desorption from the intrinsic and extrinsic precursors are very similar we set $S_0^{(i)} = S_0^{(e)}$ and equate the desorption rate constants out of these states, $r_i(T) = r_e(T)$, to get

$$S_t^{(\mathrm{prec})}(\theta,T) = S_0^{(t)}(T)\frac{r_{c\leftarrow i}^{(t)}(\theta,T)(1-\theta)}{r_{c\leftarrow i}^{(t)}(\theta,T)(1-\theta) + r_i(T)} \tag{24}$$

$r_{c\leftarrow i}^{(t)}(\theta,T)$ and $r_{c\leftarrow e}^{(t)}(\theta,T)$ are the rates of conversion from the precursors into the chemisorbed state localized at a top site. Their coverage dependence is dictated by the local environment into which the particle must accommodate. To a good approximation this is the same as what a particle sees in direct adsorption except that, for the transition from the intrinsic precursor, an empty site is guaranteed. Thus we may write for the coverage dependence of the conversion rates

$$r_{c\leftarrow i}^{(t)}(\theta,T) = w_{c\leftarrow i}^{(t)}(T)S_t(\theta,T)/[S_0^{(t)}(T)(1-\theta)] \tag{25}$$

$$r_{c\leftarrow e}^{(t)}(\theta,T) = w_{c\leftarrow e}^{(t)}(T)S_t(\theta,T)/S_0^{(t)}(T) \tag{26}$$

For the rate constant of conversion we postulate a simple Arrhenius form

$$w_{c\leftarrow i}^{(t)} = \nu_{ci}^{(t)}\exp[-Q_{ci}^{(t)}/k_B T] \tag{27}$$

so that, for mobile precursors, we obtain

$$\frac{r_i}{w_{c\leftarrow i}^{(t)}} = \frac{v_i}{v_{ci}^{(t)}} \exp[-(V_i - Q_{ci}^{(t)})/k_B T] \tag{28}$$

where v_i is the frequency of vibration of a particle in the intrinsic precursor state, perpendicular to the surface and V_i is its binding energy. A similar expression holds for the bridge sites. This simplifies the precursor-mediated sticking to a transparent form

$$S_t^{(prec)}(\theta, T) = S_0^{(t)}(T) \times \frac{S_t(\theta, T)/S_0^{(t)}(T)}{S_t(\theta, T)/S_0^{(t)}(T) + r_i/w_{c\leftarrow i}^{(t)}} \tag{29}$$

and similarly for sticking into the bridge sites, $S_b^{(prec)}$.

We have studied the adsorption kinetics by measuring the time evolution of the partial coverages for several temperatures and pressures [20]. We are now in a position to calculate this time evolution by solving (15) and (16), in the absence of desorption, with the sticking coefficients given by (29). For fast surface diffusion and site conversion we do this by summing these equations and solving for $\theta(t) = \theta_t(t) + \theta_b(t)$. If we assume, reasonably, that $w_{c\leftarrow i}^{(t)} = w_{c\leftarrow i}^{(b)}$ then we only have one additional parameter, given by (28), to describe the adsorption kinetics. This parameter must be small compared to the sticking at low coverage to yield a constant sticking at low temperatures and the activation barrier in (28) must be of order $k_B T_{ha}$, to allow some temperature dependence of the evolution.

A fit to the time evolution of the partial coverages also requires the knowledge of the flux of the incoming particle beam, i.e. its effective temperature and effective pressure. Both are poorly defined for a non-thermal beam. However, the kinetic energy of the beam of 90 meV is equivalent to a temperature of 500 K and the pressure is determined from an uncalibrated ion gauge, with a systematic uncertainty of a factor of two.

In Fig. 7 we show the time evolution, measured and calculated, for four surface temperatures. The coverages rise monotonically to 1/2 ML with the bridge coverages trailing due to their lower binding energy. Also, the approximately linear rise of the top site coverage implies a constant top-site sticking coefficient, initially. This makes the fitting of the low coverage evolution straightforward, namely, the factor (28) must be negligible so that only one number, the product of the constant initial sticking and the flux, determines the slope. Standard coverage-dose curve analyses give estimates of S_0 in the range 0.5–0.9 and with little temperature dependence [1,4,21,22,44]. If we settle on the most common value of $S_0 = 0.85$ and use the experimentally estimated pressures then all initial slopes are too low by about a factor of two, which is within the mentioned uncertainty.

Having fitted the initial slope we then adjust the prefactor and activation energy in (28) to get an overall fit to both partial coverages at all temperatures (including several isotherms not shown here). The agreement between theory and experiment, on the basis of the implementation of our model with the fewest number of parameters, is very good. Above 1/2 ML at lowest temperatures, we have not tried to reproduce the small but finite adsorption rate. We recall from the fitting of equilibrium partial coverages that variations around half a monolayer are sensitive to the small longer ranged interactions. This has a marked effect on the magnitude of the sticking coefficients in this regime: On top of the dramatic decrease at 1/2 ML due to the large first neighbor repulsions, by two orders of magnitude at 200 K, come variations of an order of magnitude or so due to the smaller interactions. Yet this small sticking coefficient is responsible for the slow further increase of the coverage with time. We remark that the parameters in the precursor rate factor (28) are physically reasonable with $V_i - Q_{ci}^{(t)} \simeq 600$ K.

In Fig. 8 we show the resulting, normalized, site- and total precursor-mediated and direct sticking coefficients as a function of coverage and for two temperatures in the adsorption range (panels a and b) and two in the desorption range (panels c and d). The latter two have not been fitted but are our prediction; such as these are needed to calculate the desorption kinetics. Features of the low-temperature sticking mimick those of the chemical potential, even in the precursor form, and for the same reasons. Thus there are inflections and plateaus just below 1/2 ML, corresponding to the onset of the ordering into the $c(4 \times 2)$ structure, and precipi-

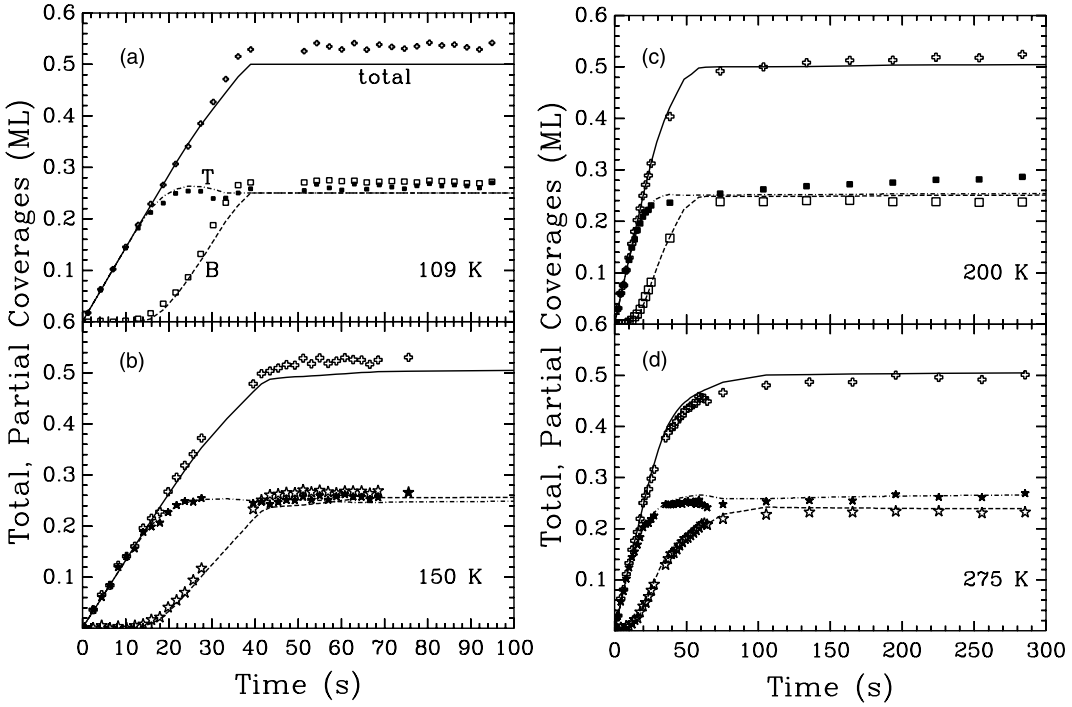

Fig. 7. The evolution of site coverages in adsorption at four substrate temperatures measured in XPS: top-site (filled symbols), bridge-site (open) and total coverage (crosses); gas pressure 3×10^{-8} Torr. The corresponding theoretical curves are obtained with the precursor-mediated sticking coefficients (cf. Fig. 8) calculated for our standard parameters of Fig. 3 and precursor rate factors $\nu_i/\nu_{ci}^{(a)} = 0.1$, $(V_i - Q_{ci}^{(a)})/k_B = 600$ K, $a = t$, b.

tous drops at 1/2 ML. However, because all our interactions, including first neighbor, are finite, the decrease in the sticking coefficients (direct and precursor-mediated) is less dramatic at elevated temperatures. We remark that similar inflections of precursor-mediated sticking have been measured directly for the systems CO/Ru(0 0 0 1) and CO/Cu(1 1 1) [45] where ordering induced by lateral repulsion occurs at low temperature.

In principle we do not have to model the time evolution in adsorption to see the features in the total sticking coefficient, exhibited in Fig. 8(a) and (b); we can take a derivative of the total coverage vs. time curves as provided in the experiment, directly. However, this procedure is numerically difficult because of experimental conditions, such as fluctuations or gaps in the data record, and is best done by fitting a continuous curve to the data. We have done this in three ways: (i) by performing a running average, (ii) by a least squares fit to an analytic form, and (iii) by matching limiting forms for $\theta(t)$, for short and long times, to spline interpolants constructed in between. In Fig. 9 we show these fits to the coverage curve at 275 K and the resulting sticking coefficient. The constant-sticking region extends to about 0.3 ML. At lower temperatures e.g. 150 K, this runs to 0.4 ML, i.e. about twice the range that other analyses of other exposure curves have produced [1,4,21]. We also show our theoretical result, at 275 K, which is in good agreement with the derivative results, considering the uncertainties in the latter.

5. Desorption kinetics

In the temperature range of desorption we can safely assume that rates of hopping and surface diffusion are much faster than rates of desorption. This implies that during desorption the adsorbate is maintained in thermal equilibrium at the instantaneous temperature, $T(t)$, and coverage, $\theta(t)$

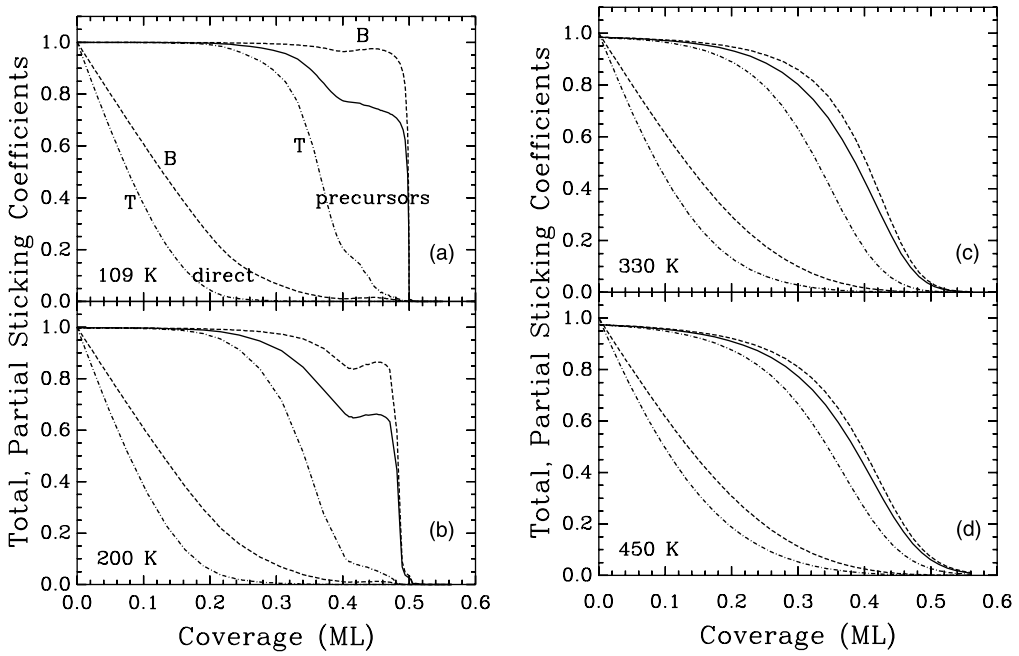

Fig. 8. Precursor-mediated (upper right curves) and direct (lower left) sticking coefficients for top sites (dash-dotted lines), bridge sites (dashed) and their total (solid) for standard parameters and temperatures, panel (a) $T = 109$ K, (b) 200 K, (c) 330 K, (d) 450 K.

with the partial coverages given by their equilibrium values, $\theta_t(t) = \theta_t(\theta(t), T(t))$ and $\theta_b = \theta - \theta_t$. Thus the only macroscopic variable in the system during desorption is the total coverage, θ, and the kinetics are given by [35]

$$\left.\frac{d\theta}{dt}\right|_{des} = -S(\theta,T)\frac{a_s}{\lambda_{th}^2}\frac{k_B T}{h} Z_{int}\exp[\mu_{ad}(\theta,T)/k_B T] \tag{30}$$

where $S(\theta, T)$ is the sticking coefficient, a_s is the area of a surface unit cell; Z_{int} and λ_{th} appear in Section 3.1. We again express the adsorbate chemical potential $\mu_{ad}(\theta, T)$ as a sum of contributions, as in (12), to get for the rate of desorption

$$R_d = S(\theta,T)\frac{\theta}{1-\theta}\frac{a_s}{\lambda_{th}^2}\frac{k_B T}{h}\frac{Z_{int}}{q_3^{(t)} q_{int}^{(t)}} e^{-V_0^{(t)}/k_B T} e^{\mu_{lat}/k_B T} \tag{31}$$

The commonly assumed form for this rate, namely, a product of a temperature-dependent rate constant and a factor of θ, follows with the assumption of simple site-blocking sticking, $S(\theta) = 1 - \theta$, and no interactions, $\mu_{lat} = 0$. The occurrence of exclusions between top and bridge sites, alone, already requires a proper evaluation of the sticking [42]. Significant first neighbor interactions, in addition, demand that both S and μ_{lat} be evaluated within the one model. Although one can estimate such interactions by a fit to experimental desorption data alone, this nevertheless requires assumptions about the coverage and temperature dependence of the sticking coefficient, as this is seldom determined by experiment *in the desorption range*. However, here we are in the ideal situation of having determined all quantities in (31) by our previous fits to the equilibrium and adsorption data, so that a direct test of the model interactions is obtained by comparing the TPD spectra as calculated from (31) with good experimental data [1,26].

In Fig. 10(a) we show the TPD spectra calculated with the binding and interaction parameters used to fit the pressure isotherms, Fig. 4(a). It is clear that the CO repulsive energy is too large, i.e. it shifts the leading edges and peaks to too low temperatures, even at the lowest initial coverages.

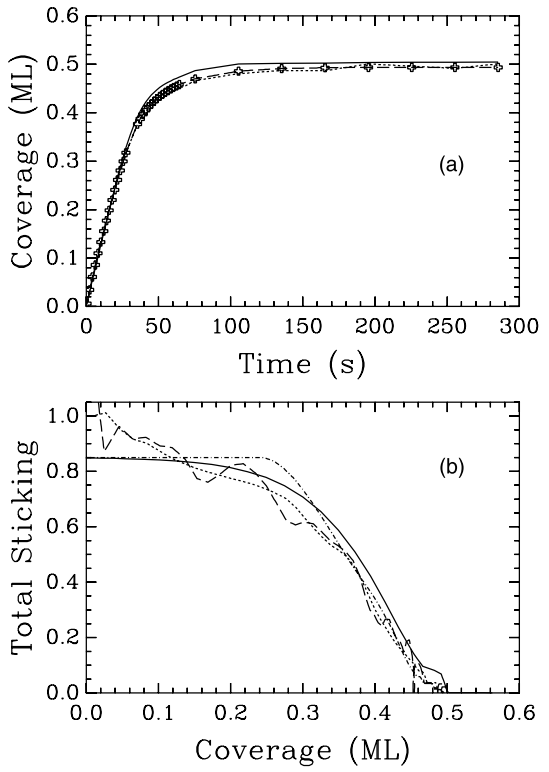

Fig. 9. Curve fits to the measured total coverage (crosses, panel a) and the derived total sticking (panel b) for $T = 275$ K. The procedures (i)–(iii) described in the text correspond to the long-dashed, dotted, dash-dotted lines, respectively. The calculated coverage and sticking is shown as the solid line (cf. Fig. 7(d)).

This can be rectified by simply reducing the mean field interaction, $V_{mf} = 40$ kJ/mol/ML, invoked for this fit. In Fig. 10(b) we show the results obtained by almost halving V_{mf} to get an excellent fit to the data. (This amounts to a reduction of μ_{lat}—due to short range and mean-field interactions—by about 20% at the lowest desorption temperatures/highest initial coverages.)

Thus there appears to be some discrepancy between the modeling of the equilibrium pressure data (which were only measured below 0.14 ML but at desorption temperatures) and the TPD data. To confirm this discrepancy we compare our model rate predictions (with $V_{mf} = 22.5$ kJ/mol/ML), without further adjustment, with a second data set, Fig. 10(c). For initial coverages below 1/2 ML the agreement is again very good, with regard to both peak positions and width. (Note: The Pt surface in this experiment has a small concentration of defects which we have not included and which binds CO more strongly, generating a higher trailing edge. In any case there is also some experimental uncertainty; for example, intersecting desorption traces in the trailing edges of both data sets.) The differences between calculated and measured rates in Fig. 10(c) for initial coverages larger than 1/2 ML are directly attributable to the behaviour of the sticking in this region. As discussed earlier this region is difficult to model and we have made no special effort here. If we simply increase the tiny sticking, in this region, by a factor of 2–3, we eliminate most of the overshoot in the model rates against the two highest experimental traces and, moreover, recover the local minima which these exhibit.

This smaller mean field interaction energy produces a heat of adsorption, in the desorption temperature range, with an initial slope of 51 kJ/mol/ML, a 30% reduction of Poelsema et al.'s data fitting value, and which decreases roughly linearly with coverage. Other estimates range from 37 kJ/mol/ML [44], 49 kJ/mol/ML [4,21] to Yeo et al.'s [19] large value of roughly 75 kJ/mol/ML. As possible origins of this discrepancy in the mean field contribution one should reconsider the calibration of the scattering intensity vs. coverage curves. In particular, the assumption of a random distribution of CO molecules is suspect at the higher coverages sampled by Poelsema et al.. We note that the result obtained by Yeo et al. is clearly at odds with the TPD spectra. Their low-coverage value of the heat of adsorption (180 kJ/mol) implies a peak to the desorption spectra at about 630 K instead of 470 K as observed; their large decrease of Q_{iso} with coverage implies much broader spectra.

For completeness we have performed an Arrhenius analysis of our model TPD spectra (that fit the experimental data). This parameterization defines a coverage- and temperature-dependent desorption energy

$$E_d(\theta, T) = -\left.\frac{\partial(\ln R_d)}{\partial\beta}\right|_\theta \tag{32}$$

$$= Q_{iso}(\theta, T) - \frac{k_B T}{2} - \left.\frac{\partial[\ln S(\theta, T)]}{\partial\beta}\right|_\theta \tag{33}$$

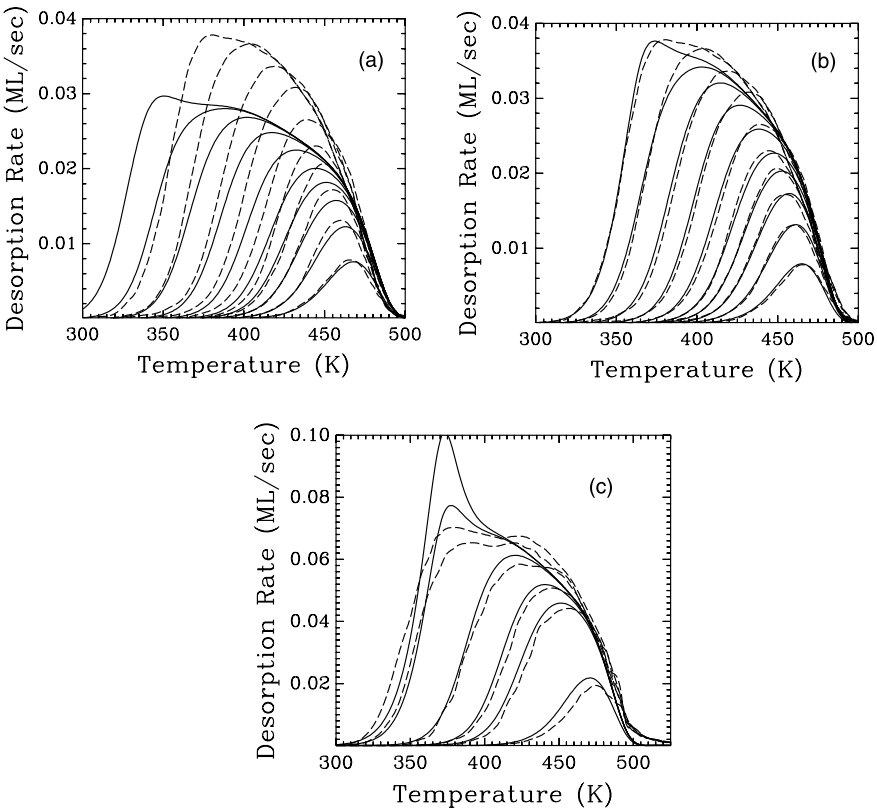

Fig. 10. (a) Comparison of TPD spectra, theory (solid lines) for the model parameters applicable to the solid lines of Fig. 4(a) and measured (dashed lines, from [26]). Sticking of the form of Fig. 8(c) and (d) with $S_0 = 0.85$. Heating rate 8 K/s, initial coverages 0.04, 0.07, 0.1, 0.13, 0.16, 0.21, 0.27, 0.34, 0.42, 0.50 ML. (b) as (a) but top-site binding and mean-field interaction energies adjusted to $V_0^{(t)} = 148.8$ kJ/mol and $V_{mf} = 22.5$ kJ/mol/ML. (c) Comparison of rates calculated (solid lines), for the same interaction and sticking parameters as (b), and measured (dashed lines, from [1]). Heating rate 15.5 K/s, initial coverages 0.06, 0.18, 0.24, 0.35, 0.52, 0.58 ML.

where the second line follows from the equality of adsorption and desorption rates in equilibrium. This desorption energy, averaged over the desorption temperature range, is shown in Fig. 4(c) (dashed line). At low coverages the last term in (33) is negligible and $E_d(\theta)$ follows the corresponding averaged heat of adsorption to within $k_B T_{des}/2$. However, as coverage increases the precursor rate factor in (29) comes into play so that, by 1/2 ML, $E_d(\theta)$ has dropped below Q_{iso} by an additional amount proportional to the precursor rate barrier and considerably below the low-temperature-averaged $Q_{iso}(\theta, T)$ (solid line). Thus erroneous comparisons of results for "desorption energy" with "heat of adsorption" must naturally produce disagreement for this system, even with ideal experimental data. We also show the resulting temperature-averaged prefactor in Fig. 4(c). It is roughly constant up to 0.3 ML, with a value of about 3×10^{15} s^{-1}, a typical value of CO on transition and noble metals. Beyond this, it drops by a factor of 10 at 1/2 ML as a direct consequence of the reduction in the total sticking coefficient.

Kinne et al. [20] have also measured isothermal desorption traces for low to moderate initial coverages and high temperatures. In Fig. 11(a) we show as dashed lines the time evolution of the coverage, generated for the parameters which well fit the TPD data, Fig. 10(b). Apparently, the experimental isothermal rates are too slow (i.e. coverages remain too large), thus in contradiction to the experimental TPD data. Indeed, if we were to

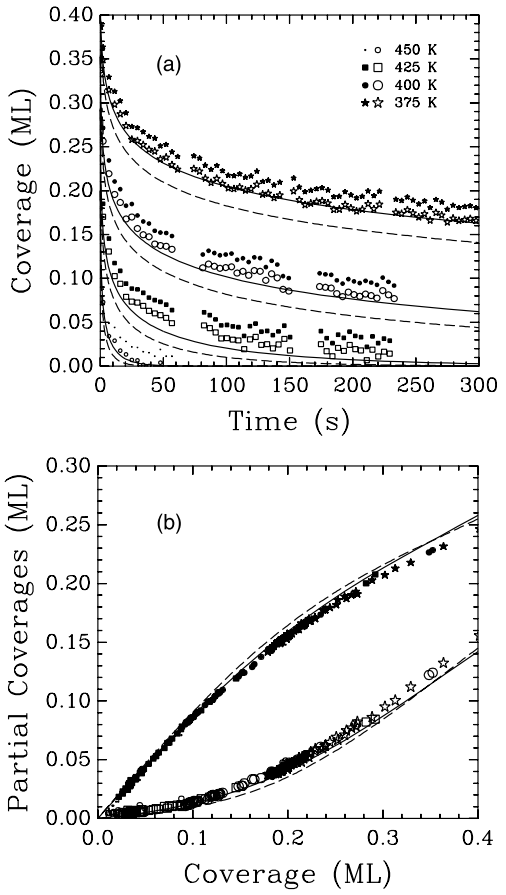

Fig. 11. (a) Comparison of calculated (lines) and measured (symbols) isothermal desorption traces with allowance for experimental uncertainties. Data from [20] (filled symbols) and modified by subtraction of 0.015 ML (open symbols). Calculated values assume the parameters of Fig. 10(b) for the stated temperatures (dashed lines) and these values reduced by 5 K (solid). (b) Partial coverage vs. coverage plots for all the data in (a) and calculated for $T = 330$ K (dashed) and $T = 450$ K (solid).

take the low coverage rates from these isothermal experiments we would find that the corresponding TPD peaks would be upshifted by 16 K. This corresponds to a binding energy change of about 700 K, not within any experimental error. The discrepancy in Fig. 11(a) is not an indication that our model is incorrect for, as we show in Fig. 11(b), the predicted partial coverage vs. coverage plots follow the experimental data well, as indeed they should. The discrepancy can be removed if one allows as little as one per cent, or so, of surface defects that constitute more strongly bound adsorption sites, and a similar relative error in temperature control, both magnitudes being within the uncertainty of this experiment. Removing defects by subtracting 0.015 ML from the experimental coverages and decreasing our model temperatures by 5 K we get not only a fair fit between our theory and the (modified) isothermal traces but also consistency between isothermal and TPD data.

6. Discussion

To account for and to understand not only the main features but also the details of the CO/Pt(1 1 1) system, a comprehensive theory must account for (i) the geometry, (ii) the energetics and (iii) the kinetics of the system. The first is done by including several adsorption sites per unit surface cell, in particular on-top and bridge sites. The second demands the specification of different binding energies on the different sites, a multitude of short- and long-ranged lateral interactions, and a number of vibrational/rotational modes and frequencies. To do this we have developed a multi-site lattice gas model. To deal with the kinetics we have extended this to the kinetic multi-site lattice gas model. The model contains a number of parameters, some of which (such as the vibrational frequencies) are known from independent experiments; all of these parameters can, at least in principle, be determined by ab initio quantum mechanical calculations, density functional theory or otherwise.

Once the model has been specified one must use it to reproduce and understand a large set of diverse experimental results on equilibrium data (adsorption isotherms, heat of adsorption, partial coverages, phase diagram and ordered structures) and on kinetic data (sticking coefficients and thermal desorption rates). All these data represent functions of temperature and coverage and the challenge to theory is to reproduce all these functions with a minimal set of parameters to adjust. The task is further complicated by the fact that some of the experimental data are contradictory and controversial.

Why is such a considerable theoretical effort desirable and even necessary? The answer is that only a comprehensive theory of all data can reduce the complexity of the adsorbate system to a few key ideas. Also, only a comprehensive theory can uncover inconsistencies in the experimental data and provide a unified picture that simpler phenomenological models of subsets of data cannot; this does not imply that the latter are not useful tools in the initial stages of discovery, to parameterize data and suggest interpretations. We discuss some deficiencies of these other models now.

To understand the low coverage pressure isotherms a model was worked out that accounts for adsorption on top sites only and treats the energetics in a mean field approximation [18]. However, occupation of the less favored bridge sites in the temperature range of the isotherms, above 400 K, is not negligible and amounts, at the highest coverage determined (0.14 ML), to about 30%. By neglecting bridge site occupation, this model ignores entropy contributions of the order of $k_B \ln 4$ (for 1 on-top and 3 bridge sites), or $\Delta E/k_B \approx 600$ K/ML at $T = 400$ K, to the free energy of the adsorbate, about 8% of their mean field energy. A further, albeit less significant, neglect of entropy in the model is the assumption of constant partition function ratios, i.e. temperature independent prefactor. The "perfect" agreement between the model and the experimental data is therefore artificial and mainly due to the facts that the low coverage, high temperature pressure isotherms are mathematically rather simple curves and can be fitted well with two parameters at one's disposal. We iterate that the energetic parameters of this model lead to low initial coverage TPD traces (in the same temperature range) with peak positions that are too low in temperature.

A later analysis of these same pressure isotherms used a lattice gas model to determine interactions out to fourth neighbours on top sites [46]. Bridge occupation was discounted, based in part on experiments which showed that only top sites were occupied to 1/3 ML. Correspondingly, for low coverages, Skelton et al. simplified their calculations by assuming an infinite first neighbor repulsion, $V_1^{(tt)}$, and proceeded to show that a non-monotonic behaviour of the interactions, $V_n^{(tt)}$, $n = 2$–4, could fit the data. We find that variations of our short-range interactions and the site-binding difference, in both calculation schemes of Table 2, do not reproduce the early stages of the partial coverage curves of Fig. 3 with $(V_2^{(tt)}, V_4^{(tt)}) < V_3^{(tt)}$. In any event, $V_1^{(tt)}$ cannot be regarded as 'infinite' at 400 K. A motivation for the non-monotonic interactions lies in the real-space superstructures proposed by Tüshaus et al. [3], for top site occupancy alone, to explain the $(\sqrt{3} \times \sqrt{3})R30°$ LEED patterns observed near 0.19 and 0.30 ML at 125 K. However, we observe finite bridge coverages, certainly at 0.3 ML.

To understand the partial coverage curves a simple model based on on-top and bridge partial coverages was advanced [15,20], in which details of lateral interactions were ignored and the gross behaviour of these coverages summarily accounted for by restricting them to a maximum value of 1/4 ML. The latter assumption denies the formation of any $\sqrt{3} \times \sqrt{3}$ structure for on-top sites at lowest temperatures. The model is characterized by a Boltzmann factor involving the free energy difference between top and bridge sites. Analysis of the data with such a model shows that this factor does not have a simple Arrhenius form. However, if the latter is assumed, together with a constant prefactor and a constant energy difference, the model reproduces the gross features of the partial coverage curves over a limited temperature range; but it cannot explain observations, such as the small overshoot of θ_t above 1/4 ML at low temperature, around $\theta = 1/3$ ML, and features around 1/2 ML. Again, with such a phenomenological model the values of the parameters extracted indicate little about the complicated energetics of the system.

A relatively complicated model of the system, based on measurements of the stretching mode of adsorbed CO, has been constructed by Schweizer et al. [12], and used by Persson [47] to model CO phases around 1/2 ML, for example. With a one-dimensional model of the occupancy of top and bridge sites, but with incomplete top-bridge site exclusion, they use the vibrational data to determine an effective binding energy difference. They find that it decreases with increasing coverage, turning negative at low coverages, e.g. by 0.3 ML

at 200 K. They extrapolate to zero coverage for a difference of 60 meV, for a range of temperatures. Apart from the fact that these results will fail to explain the data of Fig. 3, the model disregards the inherent electronic contribution to this binding difference. A potential energy surface for top and bridge sites is constructed, based in part on experimental heats of adsorption and an assumed interaction potential for adsorbed CO. With the introduction of an off-center top site, this is used by Persson to explain low temperature compressed structures, for example. However, the calculated coverage variation of the CO binding energy, over half a monolayer, fails to reproduce the TPD spectra and the low temperature behavior of the chemical potential.

To re-emphasize the importance of a complete analysis of an adsorption system, we remark that inspection of the TPD spectra would suggest that the significant peak shifts and the lack of structure, i.e. secondary peaks due to short-ranged interactions, is a consequence of the dominance of a mean field interaction. Naively one might then be tempted to model the system as having only one binding site, as Poelsema et al. did at low coverages. Indeed, such a model with an assumed sticking coefficient of the form of Fig. 8(c) and (d)—or even a constant sticking—and an adjustable mean field parameter gives a fit to the TPD spectra of the same quality as Fig. 10(b). Nevertheless, such an approach completely misses and actually misrepresents the essential structural and energetic features of CO on Pt(1 1 1). Again, the usefulness and consistency of such fits are debatable; the sticking coefficient is not of simple form, by any means, except at the lowest initial coverages, and the lateral interactions are multiple and complex. It is therefore not surprising that the site binding energy and the mean field interaction, extracted in previous modeling of temperature-programmed and isothermal desorption data, do not reproduce other data in the same temperature range.

To re-state the obvious, a comprehensive theory as presented in this paper, although considerably more involved, is the only route to understand the complete body of experimental data, both equilibrium and kinetic. It also represents a tool to uncover and clarify inconsistencies in the data and, on a very positive note, to point out the problems to be overcome in future experimental and theoretical work.

There are several aspects of the present theory that can and should be explored and refined. As for structural properties we know from trials that small changes in some of the lateral interactions will change the overshoot of the top-site coverage at 1/3 ML, and hence the extent of the $(\sqrt{3}\times\sqrt{3})R30^\circ$ order. Simultaneous measurements of low coverage structures and partial coverages on ultraclean surfaces should resolve the inconsistencies of the data while allowing some fine tuning of the parameters.

So far our theory is restricted to coverages below those where compressional effects play a role in ordering. Presently we only see partial ordering into the structures observed above 1/2 ML. One result of the compression is that the on-top CO becomes tilted from the surface normal, as inferred by ESDIAD measurements [48]. To include such effects properly we must extend the lattice gas to a multi-site and multi-state model, as has been done for N_2/Ni(1 1 0) [49]. These new compressional phase orderings would then show up in addition to the $c(4\times 2)$ structure below 275 K which the present model already produces successfully. The additional insight thus gained will also be of consequence for the behaviour of the heat of adsorption beyond 1/2 ML; and the precise value of the "small" sticking coefficient there, which controls secondary features of the adsorption and desorption kinetics.

Acknowledgements

The work at Dalhousie was supported by grants from NSERC and the US Office of Naval Research.

Appendix A

In this appendix we demonstrate that complete nearest neighbor same-site exclusion, as well as top-bridge exclusion within cells, gives equal

occupancy of top and bridge sites at saturation. We use a one-dimensional model with two sites for which analytical results are known. The partial coverages are given by

$$\theta_t = \frac{1+x-2\theta y}{2(1-x)} \times \left[1-\left\{1-4(1-x)\frac{\theta(1-\theta)}{(1+x-2\theta y)^2}\right\}^{1/2}\right] = \theta-\theta_b \quad (A.1)$$

where

$$x = \exp[\beta(E_t - E_b)] = \frac{q_3^{(b)} q_{int}^{(b)}}{q_3^{(t)} q_{int}^{(t)}} \exp\left[-\beta\left(V_0^{(t)} - V_0^{(b)}\right)\right] \quad (A.2)$$

In the absence of interactions to nearest neighbor sites, $V_1^{(tt)} = V_1^{(bb)} = 0$, we have $y = 1$ and the partial coverages at $\theta = 1$ are zero and one for the weaker and stronger bound sites, respectively, see Fig. 12, dashed lines. Nearest neighbor site exclusion, $V_1^{(tt)}$, $V_1^{(bb)}$ both infinite, gives $y = x$ and results in equal top and bridge site populations at a saturation coverage of 2/3 ML with the following structure,

$$|\blacklozenge\square|\diamondsuit\blacksquare|\diamondsuit\square|\blacklozenge\square|\diamondsuit\blacksquare|\diamondsuit\square|\blacklozenge\square|\diamondsuit\blacksquare|\diamondsuit\square| \quad (A.3)$$

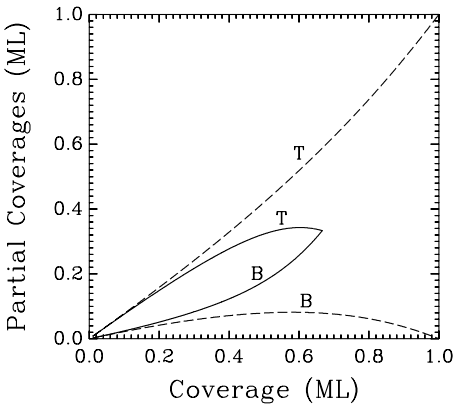

Fig. 12. Partial coverages of top and bridge sites in the absence of nearest neighbor repulsions (dashed lines) and in the presence of infinite repulsion (solid lines) in a one-dimensional system. The relative binding of top and bridge sites is fixed with $x = 0.3$ in (A.2).

where we have represented bridge and top site occupation, within a cell, by a filled square or diamond, respectively. An example of partial coverages is given in Fig. 12. Note that on an hexagonal lattice the saturation coverage is 1/2 ML in this case.

For completeness we also list the direct sticking coefficients for top and bridge sites in this case,

$$S_t(\theta_t,\theta_b,T)/S_0^{(t)}(T) = \frac{(1-2\theta_t-\theta_b)^2(1-2\theta_b-\theta_t)}{(1-\theta)^2} \quad (A.4)$$

$$S_b(\theta_t,\theta_b,T)/S_0^{(b)}(T) = \frac{(1-2\theta_t-\theta_b)(1-2\theta_b-\theta_t)^2}{(1-\theta)^2} \quad (A.5)$$

More details can be found in [42].

References

[1] H. Steininger, S. Lehwald, H. Ibach, Surf. Sci. 123 (1982) 264.
[2] B. Poelsema, R.L. Palmer, G. Comsa, Surf. Sci. 123 (1982) 152.
[3] M. Tüshaus, E. Schweizer, P. Hollins, A.M. Bradshaw, J. Electron Spectrosc. 44 (1987) 305.
[4] G. Ertl, M. Neumann, K.M. Streit, Surf. Sci. 64 (1977) 393.
[5] H. Hopster, H. Ibach, Surf. Sci. 77 (1978) 109.
[6] J.C. Tracy, P.W. Palmberg, J. Chem. Phys. 51 (1969) 4852.
[7] N. Avery, J. Chem. Phys. 74 (1981) 4202.
[8] J.P. Biberion, M.A. van Hove, Surf. Sci. 118 (1982) 361.
[9] W.D. Mieher, L.J. Whitman, W. Ho, J. Chem. Phys. 91 (1989) 3228.
[10] B.E. Hayden, A.M. Bradshaw, Surf. Sci. 125 (1983) 787.
[11] R.G. Tobin, P.L. Richards, Surf. Sci. 179 (1987) 387.
[12] E. Schweizer, B.N.J. Persson, M. Tüshaus, D. Hoge, A.M. Bradshaw, Surf. Sci. 213 (1989) 49.
[13] H. Froitzheim, M. Schulze, Surf. Sci. 211/212 (1989) 837.
[14] G. Hähner, J.P. Toennies, Ch. Wöll, Appl. Phys. A 51 (1990) 208.
[15] A. Cudok, H. Froitzheim, M. Schulze, Phys. Rev. B 47 (1993) 13682.
[16] A.P. Graham, J. Chem. Phys. 109 (1998) 9583.
[17] H. Froitzheim, H. Hopster, H. Ibach, S. Lehwald, Appl. Phys. 13 (1977) 147.
[18] B. Poelsema, R.L. Palmer, G. Comsa, Surf. Sci. 136 (1984) 1.
[19] Y.Y. Yeo, L. Vattuone, D.A. King, J. Chem. Phys. 106 (1997) 392.
[20] M. Kinne, T. Fuhrmann, C.M. Whelan, J.F. Zhu, J. Pantförder, M. Probst, G. Held, R. Denecke, H.-P. Steinrück, J. Chem. Phys. 117 (2002) 10852.

[21] E.G. Seebauer, A.C.F. Kong, L.D. Schmidt, Surf. Sci. 176 (1986) 134.
[22] C.T. Campbell, G. Ertl, H. Kuipers, J. Segner, Surf. Sci. 107 (1981) 207.
[23] D.M. Collins, W.E. Spicer, Surf. Sci. 69 (1977) 85.
[24] P.R. Norton, J.W. Goodale, E.B. Selkirk, Surf. Sci. 83 (1979) 189.
[25] R.J. Gorte, L.D. Schmidt, Surf. Sci. 11 (1981) 260.
[26] K.-H. Allers, H. Pfnür, D. Menzel, Surf. Sci. 291 (1993) 167.
[27] B. Poelsema, L.K. Verheij, G. Comsa, Phys. Rev. Lett. 49 (1982) 1731.
[28] M. Croci, C. Félix, G. Vandoni, W. Harbich, R. Monot, Surf. Sci. Lett. 290 (1993) L667.
[29] J.E. Reutt-Robey, D.J. Doren, Y.J. Chabal, S.B. Christman, Phys. Rev. Lett. 61 (1988) 2778.
[30] J.V. Nekrylova, I. Harrison, J. Chem. Phys. 101 (1994) 1730.
[31] J.V. Nekrylova, I. Harrison, Chem. Phys. 205 (1996) 37.
[32] G. Blyholder, J. Chem. Phys. 68 (1964) 2772.
[33] P.J. Feibelmann, B. Hammer, J.K. Nørskov, F. Wagner, M. Scheffler, R. Stumpf, R. Watwe, J. Dumesic, J. Phys. Chem. B 105 (2001) 4018.
[34] D. Geschke, T. Başţuğ, T. Jacob, S. Fritzsche, W.-D. Sepp, B. Fricke, S. Varga, J. Anton, Phys. Rev. B 64 (2001) 235411.
[35] H.J. Kreuzer, S.H. Payne, Theoretical approaches to the kinetics of adsorption, desorption and reactions at surfaces, in: M. Borowko (Ed.), Computional Methods in Colloid and Interface Science, Marcel Dekker Inc., New York, 1999.
[36] D.P. Landau, K. Binder, A Guide To Monte Carlo Simulations in Statistical Physics, Cambridge University Press, Cambridge, 2000.
[37] C. Stampfl, H.J. Kreuzer, S.H. Payne, H. Pfnür, M. Scheffler, Phys. Rev. Lett. 83 (1999) 2993.
[38] S.H. Payne, H.J. Kreuzer, L.D. Roloefs, Surf. Sci. Lett. 259 (1991) 781.
[39] H. Pfnür, P. Feulner, D. Menzel, J. Chem. Phys. 79 (1983) 4613.
[40] S.H. Payne, Zhang Jun, H.J. Kreuzer, Surf. Sci. 264 (1992) 185.
[41] H.J. Kreuzer, J. Chem. Phys. 104 (1996) 9593.
[42] S.H. Payne, H.J. Kreuzer, M. Kinne, R. Denecke, H.-P. Steinrück, Surf. Sci. 513 (2002) 174.
[43] R.J. Baxter, Exactly Solved Models in Statistical Mechanics, Academic Press, New York, 1982.
[44] R.W. McCabe, L.D. Schmidt, Surf. Sci. 65 (1977) 189.
[45] S. Kneitz, J. Gemeinhardt, H.-P. Steinrück, Surf. Sci. 440 (1999) 307.
[46] D.C. Skelton, D.H. Wei, S.D. Kevan, Surf. Sci. 320 (1994) 77.
[47] B.N.J. Persson, Phys. Rev. B 40 (1989) 7115.
[48] M. Kiskinova, A. Szabó, J.T. Yates, Surf. Sci. 205 (1988) 215.
[49] H.J. Kreuzer, S.H. Payne, M. Grunze, C. Wöll, Z. Physikal. Chemie 202 (1997) 273.